

Gas Permeability Evolution with Deformation and Cracking Process in a White Marble Under Compression

Z. B. Liu^{1,2} · J. F. Shao^{1,2} · D. W. Hu³ · S. Y. Xie^{1,2}

Received: 10 July 2015 / Accepted: 12 November 2015 / Published online: 23 November 2015
© Springer Science+Business Media Dordrecht 2015

Abstract This paper presents an experimental study on the gas permeability evolution with deformation and cracking process in a white marble under compressive stresses. Uniaxial and triaxial compression tests with different confining pressures are firstly carried out to generate different states of deformation and induced cracks. The spatial distribution and geometrical form of induced cracks are investigated by the X-ray micro-tomographic imaging technique. Localized splitting-type macroscopic cracks are generated in the uniaxial test, while diffuse-oriented micro-cracks are induced in triaxial compression tests. Then, each of the cracked marble samples is subjected to a hydrostatic compression cycle, with the measurement of permeability and axial and lateral strains. It is found that the initial permeability of the sample with localized cracks is higher than that with diffuse cracks. The permeability of cracked samples exhibits an irreversible evolution between the hydrostatic loading and unloading, and the evolution trend is influenced by the initial crack state induced by the previous mechanical tests. The deformation of cracked samples under hydrostatic compression is clearly anisotropic due to oriented crack distributions and irreversible due to the unilateral closure—opening property of cracks. Finally, we propose to use the nonlinear regression method to formulate best-fitting models to capture the relationships between the permeability evolutions and effective hydrostatic stress or axial and lateral strains of cracked samples.

Keywords Permeability · Crack · Porosity · Tomography · Compaction · Marble

✉ J. F. Shao
jian-fu.shao@polytech-lille.fr

¹ College of Civil and Architecture Engineering, Hubei University of Technology, Wuhan, China

² Laboratory of Mechanics of Lille, University of Lille, 59655 Villeneuve d'Ascq, France

³ State Key Laboratory of Geomechanics and Geotechnical Engineering, Institute of Rock and Soil Mechanics, Chinese Academy of Sciences, Wuhan 430071, China

1 Introduction

Hydromechanical behavior and permeability evolution of rock masses are a major concern in many rock engineering applications. For example, in the context of the geological disposal of radioactive wastes, the sequestration of acid gas and the unconventional exploration of oil and gas, it is necessary to characterize both mechanical and hydraulic properties of host rocks. On the other hand, the cracking initiation and propagation are the main mechanism of inelastic deformation and failure in brittle rocks such as marble. The cracking affects not only the mechanical behaviors but also the transport properties such as the permeability. Indeed, in cracked rock materials, the macroscopic hydromechanical behaviors are controlled by both the intact porous rock mass and the induced cracks. In the case of rocks with very low initial permeability such as granite, marble and some hard clayey rocks, the overall permeability is even mainly governed by the spatial connectivity and aperture of cracks (Trimmer et al. 1980).

There are a number of experimental works devoted to the study of permeability evolutions in various rock materials, starting from the 1960s (Snow 1968; Jones 1975). About a decade later, the permeability of single fractures or joints in rock formations under hydrostatic stress was extensively investigated and generally estimated by using the basic cubic law (Witherspoon et al. 1980), which relates the permeability to fracture aperture. This law is still in use today in its varying forms. Then, some authors have studied effects of roughness and sample size on hydraulic properties of rock fractures (Raven and Gale 1985; Tsang and Witherspoon 1983, 1981; Nøttinger 1994). In the past decades, the permeability properties of rock or rock joints have extensively been studied through laboratory experiments subjected to confining pressure or normal stress (Li et al. 2008; Baghbanan and Jing 2008; Zhang et al. 2007; Cappa et al. 2006; Rutqvist and Stephansson 2003; Hans and Boulon 2003; Lee and Cho 2002; Pyrak-Nolte and Morris 2000; Myer 2000; Sibai et al. 1997; Henry and Sibai 1997; Boulon et al. 1993; Cornet and Morin 1997; Zimmerman and Bodvarsson 1996; Cook 1992; Li et al. 2009; Kwon et al. 2001; Berryman 1992; Selvadurai and Nguyen 1999; Nguyen and Selvadurai 1998; Selvadurai and Selvadurai 2010) and described by the cubic law relating the fractured rock permeability to the features of the apertures, such as the roughness and connectivity, aiming at well obtaining the flow characteristics of the artificially created single fractures.

More recently, the hydrostatic stress-induced permeability change in single-fractured rocks or rock mass has also been measured by different types of testing apparatus (Kishida et al. 2011; Wong et al. 2013; Zou et al. 2013; Souley et al. 2015; Selvadurai 2015). Most of the above experimental results investigated the hydromechanical behaviors of artificially created single fractures in order to well develop and validate the theoretical models for characterizing the permeability of the rock fractures. However, the coupling between the permeability evolution and mechanical behavior such as deformation and induced cracking process was not always properly taken into account. Further, the relationship between the permeability evolution and different induced cracks types (splitting or shearing cracks) was rarely investigated so far. Moreover, effects of mechanical loading history on the permeability evolution should also be studied.

The objective of the present work is then to perform a complementary laboratory study on the permeability evolution with deformation and cracking process in a typical rock with a low initial permeability, white marble. To this end, the marble samples will be first subjected to uniaxial and triaxial compression tests to generate an induced state of cracks. The spatial distributions and widths of induced cracks will be characterized by using the micro-tomographic imaging technique. Both localized splitting-type cracks and diffuse shearing cracks will be generated, respectively, from uniaxial and triaxial compression tests. Then, the various

cracked samples will be subjected to a hydrostatic loading–unloading cycle. Both axial and lateral strains as well as permeability evolution will be continuously measured during the loading and unloading phase. The induced anisotropy and unilateral effect of deformation in the cracked sample will clearly be demonstrated. The unilateral behavior of permeability evolution between the loading and unloading phases will also be determined. Finally, based on the nonlinear regression method, we will propose and compare some fitting models for estimate the permeability evolution of cracked samples as functions of stress and strains.

2 Testing Apparatus and Experimental Method

The autonomous and auto-compensated hydromechanical testing system (see Fig. 1) designed at the Laboratory of Mechanics of Lille (LML) was used to perform both mechanical tests to generate different state of cracks and hydromechanical tests with permeability measurement. The testing system consists of three independent components, respectively, for deviator stress loading, confining pressure application and interstitial pressure generation and monitoring, which are assembled around the triaxial cell. The acquisition of stresses, fluid pressure and flow rate, displacements or deformations is realized by specific transducers and recorded by a data acquisition center.

All tests were carried out in a thermally isolated small room with the constant temperature ($22 \pm 0.3 \text{ }^\circ\text{C}$) maintained by a central air conditioner in order to exclude the influence of temperature. The specimens tested in the present work were drilled in a cylindrical form with 37 mm in diameter and 74 mm in height.

Uniaxial and triaxial compression tests with two different confining pressures (2 and 10 MPas) are first performed in order to generate different states of deformation and cracking in the marble specimens. In Fig. 2, we show the axial and volumetric strains of specimens obtained in these tests. It is clearly seen that the mechanical behavior of the marble is strongly

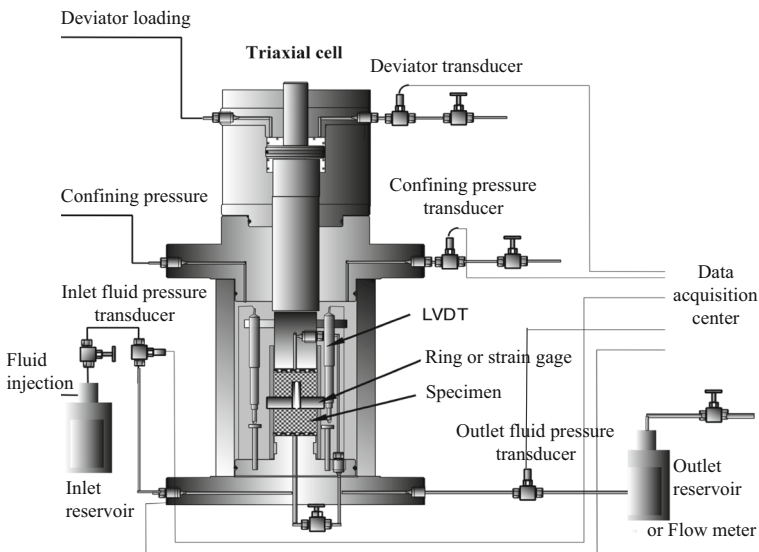


Fig. 1 Sketch of the testing apparatus for mechanical and hydromechanical tests. In steady-state method, the outlet reservoir is replaced by the flow meter

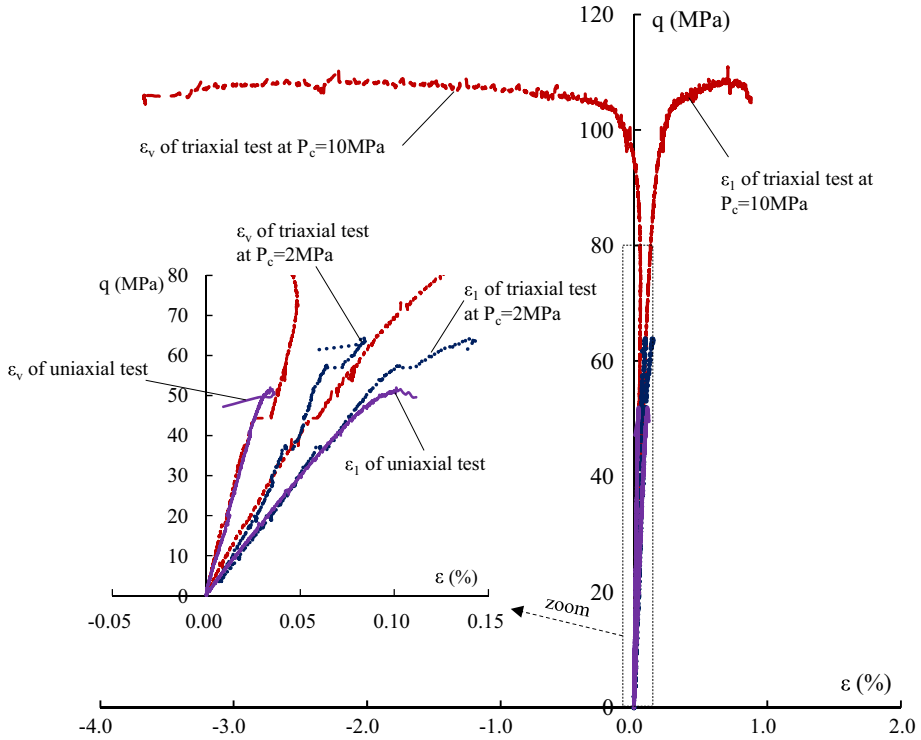


Fig. 2 Axial (ε_1) and volumetric (ε_v) strains as function of deviatoric stress (q) during uniaxial and triaxial compression tests

dependent on the applied confining pressure. In the uniaxial compression test and the triaxial compression test with the low confining pressure of 2 MPa, the strains in the marble samples remain very small (less than 0.2 %) until the failure stress is reached, and we observe a typical brittle mechanical behavior. The volume strain remains in compression until the peak stress and the relative volumetric dilation appears only in the post-peak regime due to the formation of macroscopic cracks. On the other hand, in the triaxial test with the confining pressure of 10 MPa, we observe important nonlinear strains and a progressive volumetric dilatancy before the peak stress is reached. The mechanical behavior of marble becomes significantly ductile, and the macroscopic failure of specimen appears at a large plastic deformation, for instance, about 1 % axial strain. Therefore, it is expected that strongly localized cracks are generated in the uniaxial test and triaxial test with 2 MPa confining pressures while diffuse micro-cracks in the triaxial test with 10 MPa. The distribution of generated micro-cracks and failure modes will be investigated in the next section using the technique of micro-tomography imaging.

After the preliminary tests, some hydromechanical tests are then carried out on the three cracked marbles specimens. It consists in applying hydrostatic compression cycles and measuring permeability evolutions. The objective here is to determine the correlation between permeability evolution and deformation of cracked specimens under different values of effective hydrostatic stress. The effective hydrostatic stress varies from 2 to 50 MPa. During these tests, pulse tests are performed to measure low permeability (Liu et al. 2015; Lin 1982). In the present paper, similar as the work in Trimmer et al. (1980), we report the apparent gas permeability of the fractured samples based on the cross-sectional area although discrete

fractures are created by the triaxial compression phase. Each hydromechanical test of the fractured sample is composed of the following steps:

- (1) Install the specimen in the triaxial cell, check each part of the testing apparatus to make sure it works well.
- (2) Apply the confining pressure P_c to a given level, for example, $P_c = 3$ MPa.
- (3) Inject gas into the interstitial circuit to obtain an equilibrated gas pressure P_0 at both the inlet and outlet reservoirs. We have $P_{i0} = P_{o0} = 1.0$ MPa throughout this study.
- (4) Close the valve between the inlet and outlet reservoir, apply a pressure pulse $\Delta P_{i0} = 0.1$ MPa at the inlet reservoir and cut off the gas supply. The inlet pressure P_i will decrease and the outlet pressure P_o will increase with time t .
- (5) Wait till the outlet pressure equals to the inlet pressure, i.e., $P_o = P_i = P_{end}$, and thus, a final pressure equilibrium state is obtained. With the recorded data of gas pressure decay, the rock permeability can be approximately calculated by

$$k = m \frac{\mu c L}{A} \frac{V_i V_o}{V_i + V_o} \quad (1)$$

k is the permeability in m^2 , μ and c are, respectively, the fluid dynamic viscosity and compressibility. L and A are the specimen length and cross-sectional area, while V_i and V_o are the volumes of inlet and outlet reservoirs. And m is the slope of the curve of differential pressure $\Delta P(t)$ versus time in log scale, i.e.,

$$\ln \Delta P(t) = \ln \Delta P_0 - mt \quad (2)$$

- (6) Increase the confining pressure to a new value (for example, $P'_c = 5$ MPa) and restart the procedure from the step 2) to obtain the gas pressure decay data as well as the deformation data of the specimen at the confining pressure P'_c . Increase the confining pressure step by step up to 51 MPa to realize the cracks closing phase and repeat the permeability and deformation measurement at every selected confining pressure value.
- (7) Reduce the confining pressure step by step to perform the cracks opening phase and repeat the permeability and deformation measurement at each selected confining pressure value.

To check the permeability of the intact space of the white marble, we have tested with the steady-state method by maintaining the confining stress to be 3.0 MPa and the inlet nitrogen gas to be 2.5 MPa. With a gas flow meter of measuring range from 0.004 to 0.850 ml/min, we observe no value in the flow meter. Based on this, the gas permeability of intact marble can be obtained as much lower than 10^{-20} m^2 . This value is at least 5 orders lower than the fractured sample. Thus, the permeability of the intact rock space is ignored when discussing the apparent permeability of the fractured samples.

3 X-ray Micro-tomography Imaging of Cracked Specimens

In order to characterize the distribution of cracks, the three cracked specimens are investigated using X-ray micro-tomography scanner machine. In Fig. 3, we show some selected 2D and 3D images of the cracked specimens. Due to the resolution limitation of the micro-tomographic machine for large size specimens, cracks less than micrometer cannot be visualized in the images obtained here.

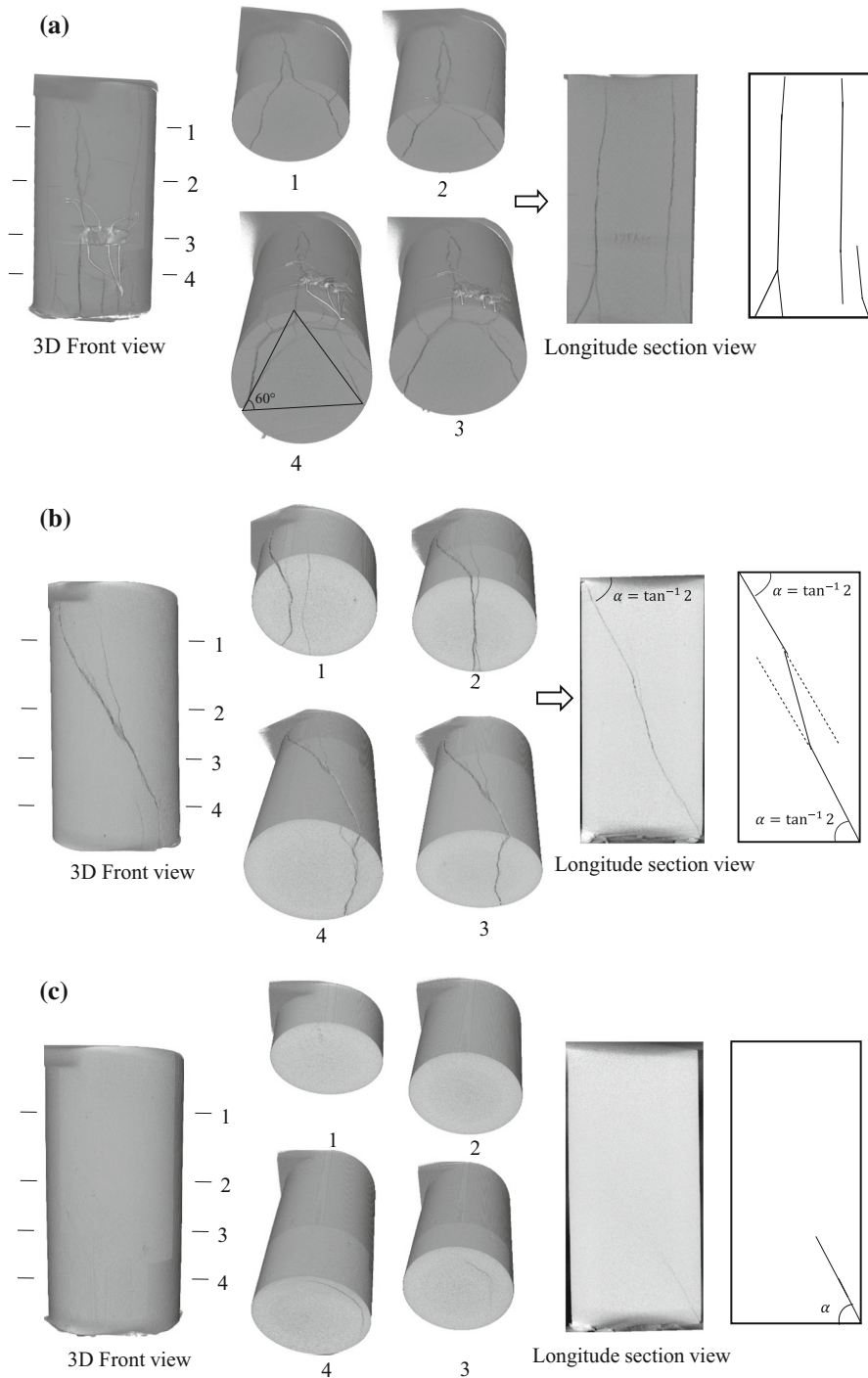


Fig. 3 X-ray micro-tomographic imaging for crack characterization of marble specimens; **a** Cracked specimen in uniaxial test; **b** Cracked specimen in triaxial test with $P_c=2$ MPa. **c** Marble tested in triaxial test with $P_c=10$ MPa

We can see in Fig. 3a that the marble sample tested in the uniaxial test shows a pair of longitudinal macroscopic cracks throughout the sample together with some randomly distributed small cracks near the sample ends of the loading position. Thus, the generated cracks propagated mainly along the major compressive stress direction in the specimen. As given by the section views in Fig. 3a, the three intersections at which the cracks intersect the sample surface approximately form an equilateral triangle. The cracks are connected from one end to the other end of the specimen. The cracks aperture is about 1–4 μm in free stress state measured by the X-ray micro-tomography image technique.

For the sample tested in the triaxial test with a confining pressure of 2 MPa (Fig. 3b), one can observe a very regular geometry at the longitude section view with the crack orientation intersecting the end surface at an angle of $\alpha \approx \tan^{-1} 2 \approx 70^\circ$. Due to the friction effect at the loading ends, the crack surface is in the form of a cone close to the specimen ends and a plan in the middle part of the specimen. The crack in the longitude section as well as in the entire specimen is generally antisymmetric to the middle cross section. And the cracks are also connected through the specimen from one end to the other, similar to the sample tested in the uniaxial test. The major crack intersects the maximum compressive stress direction of the specimen with an inclined angle, which is different from that of splitting cracks in the uniaxial test. The crack aperture is measured about 0.8–2.7 μm in free stress state by the X-ray micro-tomography image.

In a significantly different manner, the specimen tested in the triaxial test with a confining pressure of 10 MPa does not show connected cracks in the X-ray micro-tomography images. Only one local crack at one end of the specimen is observed in Fig. 3c. Other micro-cracks spread along only a quarter of the specimen height from the bottom end. The crack aperture is smaller than 0.8 μm in free stress state according to the X-ray micro-tomography image. This result is well agreed with the mechanical responses given in Fig. 2. The failure of the specimen under the confining pressure of 10 MPa is controlled rather by diffuse volumetric dilatancy than by localized macroscopic cracking.

Therefore, the crack distribution and failure mode of marble are influenced by the confining pressure in compression tests. The width of generated cracks is smaller when the confining pressure is higher.

4 Permeability Evolutions in Cracked Samples

According to the experimental procedure presented above, a hydrostatic compression loading–unloading cycle is applied to each cracked sample issued from the uniaxial and triaxial compression tests. At different selected values of effective confining pressure ranging from 2 to 50 MPa, say every 5 MPa, the gas permeability is measured by using the pulse test. Note that the loading phase leads to the progressive closure of cracks, while the unloading phase corresponds to the progressive opening of cracks. In Fig. 4, we present the evolutions of permeability as functions of effective confining pressure during the loading (closing phase) and unloading (opening phase) phases for three specimens.

From these results, three qualitative findings can easily be observed. The permeability of all three cracked specimens clearly decreases with the effective confining stress up to 50 MPa. The permeability values are different between the three types of cracked specimens under the same applied stress along all loading path. For each of three cracked samples, the permeability during loading phase (crack closing phase) is always higher than that during the unloading phase (crack opening phase). There is a sort of hysteretic loop, and it seems that

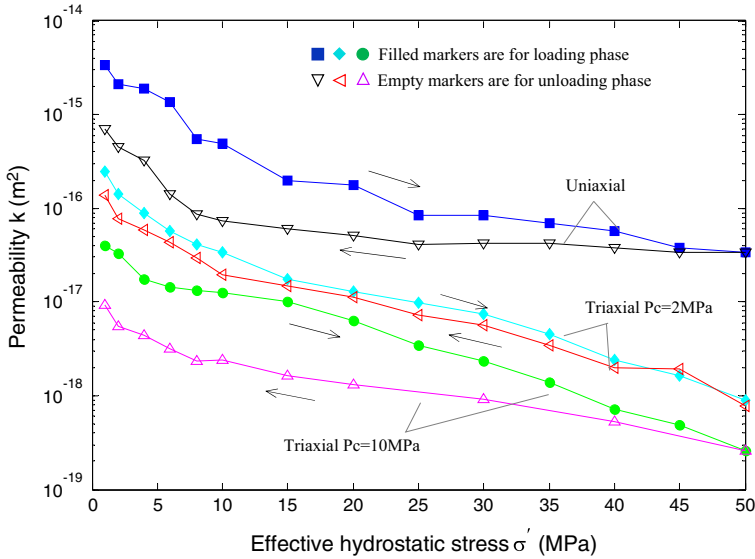


Fig. 4 Evolutions of permeability in three cracked samples during hydrostatic loading (crack closing) and unloading (crack opening) phases

the hydrostatic compression induces an irreversible closure of cracks so that the permeability is not recovered under the unloading phase.

From a quantitative point of view, depending on the applied hydrostatic stress, the permeability of the cracked marble specimen in the uniaxial test is generally in the range from $4 \times 10^{-15} \text{m}^2$ to $2 \times 10^{-17} \text{m}^2$ during the loading (crack closing) phase and from $2 \times 10^{-17} \text{m}^2$ to $7 \times 10^{-16} \text{m}^2$ during the unloading (crack opening) phase). The permeability of the cracked specimen obtained from the triaxial test with 2MPa confining pressure ranges from $2.6 \times 10^{-16} \text{m}^2$ to $9 \times 10^{-19} \text{m}^2$ in the loading phase and from $8 \times 10^{-19} \text{m}^2$ to $1.5 \times 10^{-16} \text{m}^2$ in the unloading phase. Finally, the permeability of the specimen issued from the triaxial test with 10MPa confining pressure varies from $4 \times 10^{-17} \text{m}^2$ to $2.9 \times 10^{-19} \text{m}^2$ in the loading phase and from $2.9 \times 10^{-19} \text{m}^2$ to $9.5 \times 10^{-18} \text{m}^2$ in the unloading phase. Therefore, under the effective same hydrostatic stress, the permeability of the specimen issued from the uniaxial test is approximately one order of magnitude smaller than that of the specimen from the triaxial test with 2MPa confining pressure and two orders of magnitude smaller than that of the specimen from the triaxial test with 10MPa confining pressure.

Moreover, the permeability evolution trend is also different between the three samples. As shown in Fig. 4, for the specimen issued from the uniaxial test, the permeability quickly decreases with the hydrostatic stress from 2 to 30MPa in the loading phase. When the stress is higher than 30MPa, the permeability progressively trends toward a steady value. In the unloading phase for this specimen, the permeability is nearly constant when the hydrostatic stress remains higher than 30MPa. After then, the permeability increases again quickly with the decrease in hydrostatic stress but always remains lower than its value during the loading phase for a same value of applied stress. For two other specimens issued from triaxial compression tests, even if there are similar evolution trends, there is no steady stage observed during both loading and unloading phases.

Therefore, the permeability evolution of cracked marble sample is inherently related to the state of micro-cracks induced by the preliminary uniaxial or triaxial compression tests. Under the uniaxial stress, localized macroscopic cracks are formed. The initial permeability of the cracked sample is then higher than that of the specimens with diffuse micro-cracks issued from the triaxial compression tests. Also, the permeability evolution during the hydrostatic loading and unloading is more sensitive to the applied effective stress.

5 Deformation Study of Marble

The effective permeability decrease as a result of pressure increase is in essence induced by the deformation of the fractured samples. So it is better to correlate the permeability to deformation. In Fig. 5a, b, we present the axial and lateral strains of the two cracked specimens, respectively, from the uniaxial test and triaxial test with 2 MPa confining pressure as functions of the effective hydrostatic stress during both loading and unloading phases. One

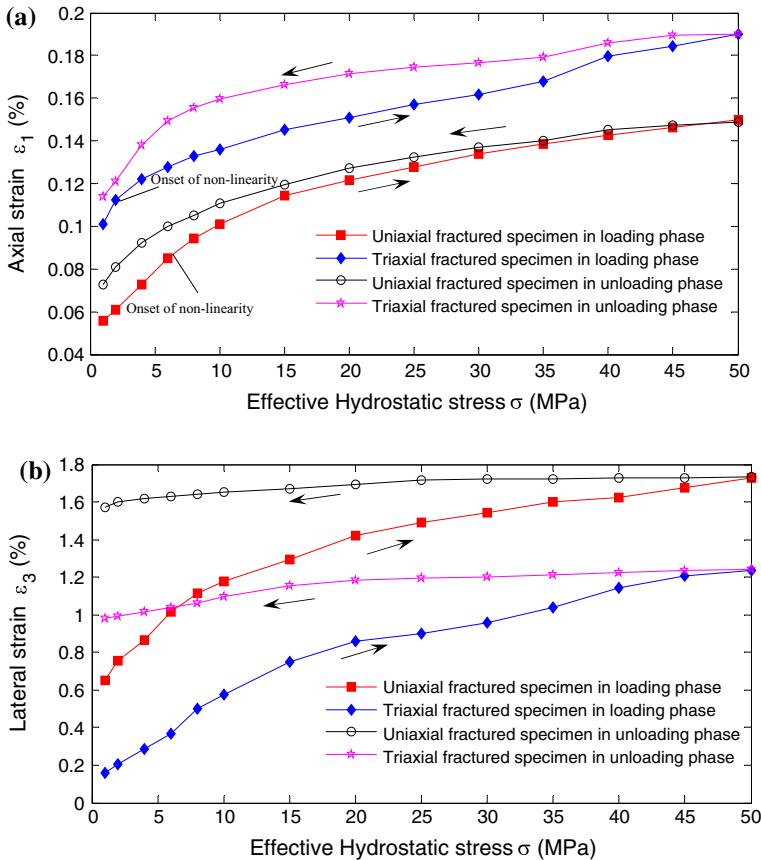


Fig. 5 Evolutions of axial strains (a) and lateral strain (b) as functions of applied effective hydrostatic stress during loading and unloading phases for two samples, respectively, cracked in uniaxial test and in triaxial test with 2 MPa confining pressure

can see that the lateral strains in Fig. 5b of both specimens are much higher than the axial strains in Fig. 5a. This means the deformations of the cracked samples are clearly anisotropic in nature due to the oriented distribution of micro-cracks and cracks. Another important phenomenon is that both axial and lateral strains exhibit an irreversible character between the loading and unloading phases. The irreversible strains are much more important for the lateral deformation than the axial one.

For more details, the axial strains of the two specimens (Fig. 5a) show a quasi-linear stress–strain relation at the beginning of the loading phase. When the applied stress exceeds a certain limit value, the specimens exhibit a typical nonlinear stress–strain behavior. The mechanical behaviors of the two specimens are qualitatively identical. However, the limit stress value for the onset of nonlinearity is higher in the specimen from the uniaxial test than that from the triaxial test. This difference can be again explained by the different states of cracks induced by the preliminary mechanical loads. Indeed, as shown in Fig. 3a, the surfaces of the major cracks of the uniaxial tested specimen are mainly parallel to the axial direction. When the specimen is subjected to a hydrostatic compression, the axial strain is rather contributed by the deformation of the intact part of specimen than the deformation of the cracks. However, for the triaxial tested specimen shown in Fig. 3b, the major cracks surfaces skew the specimen axis with an angle of $90^\circ - \alpha$. When this specimen is subjected to a hydrostatic compression, the deformation of the cracks contributes for an important part to the axial strain of the specimen. That is to say, the axial strain of the uniaxial cracked specimen is mainly due to the intact marble deformation and that of the triaxial cracked specimen is mainly due to the closing or sliding of induced cracks. As the critical stress needed for crack closure is generally smaller than that to generate nonlinear deformation of intact material, the critical stress value for the axial strain nonlinearity onset is then smaller for the uniaxial cracked specimen than for the triaxial tested one. This difference is also observed for the lateral strains in Fig. 5b even if the appearance of nonlinearity is less obvious for the lateral strains than the axial ones.

Another important result is the existence of important irreversible strains after the unloading phase. And the irreversible strain is much more important in the lateral direction than in the axial one. This phenomenon is again intimately related to the oriented distribution of cracks in the preliminary cracked samples. As more induced cracks are mainly oriented in the axial direction, the lateral strains are directly related to the progressive closure of cracks under hydrostatic stress. Due to the unilateral property of most cracks, the irreversible closure of cracks in the loading phase cannot be recovered in the unloading phase.

6 Nonlinear Regression Model of Permeability

As shown in Fig. 4, the permeability of marble is inherently related to the growth and propagation of cracks. The realistic prediction of permeability evolution with cracking process is an important issue for many engineering applications. So far, the theoretical modeling of permeability evolution taking into account cracking process is still an open issue. Thus, from a practical point of view, there is a need to formulate some experiment-based empirical models to estimate the permeability evolution in cracked rocks. In the present study, we propose to use the nonlinear regression method for the formulation of such practical permeability estimation models.

The permeability estimation models can be established by the nonlinear regression analysis in different forms, by using, for instance, the linear, exponential, logarithmic, polynomial and

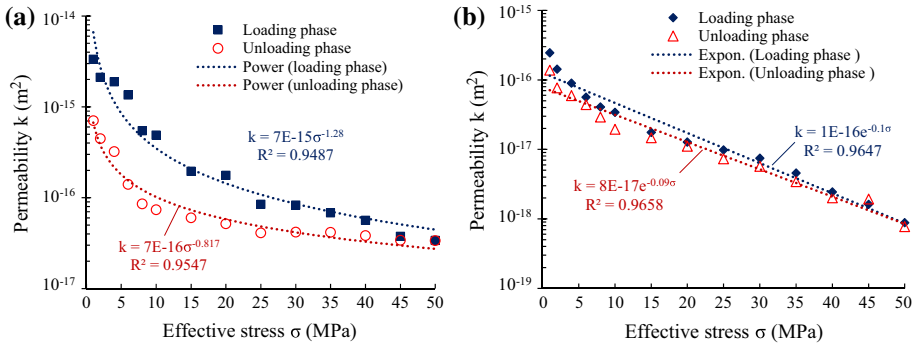


Fig. 6 Best-fitting models for permeability evolution with effective hydrostatic stress for both uniaxial cracked sample (a) and triaxial cracked sample with 2 MPa confining pressure (b)

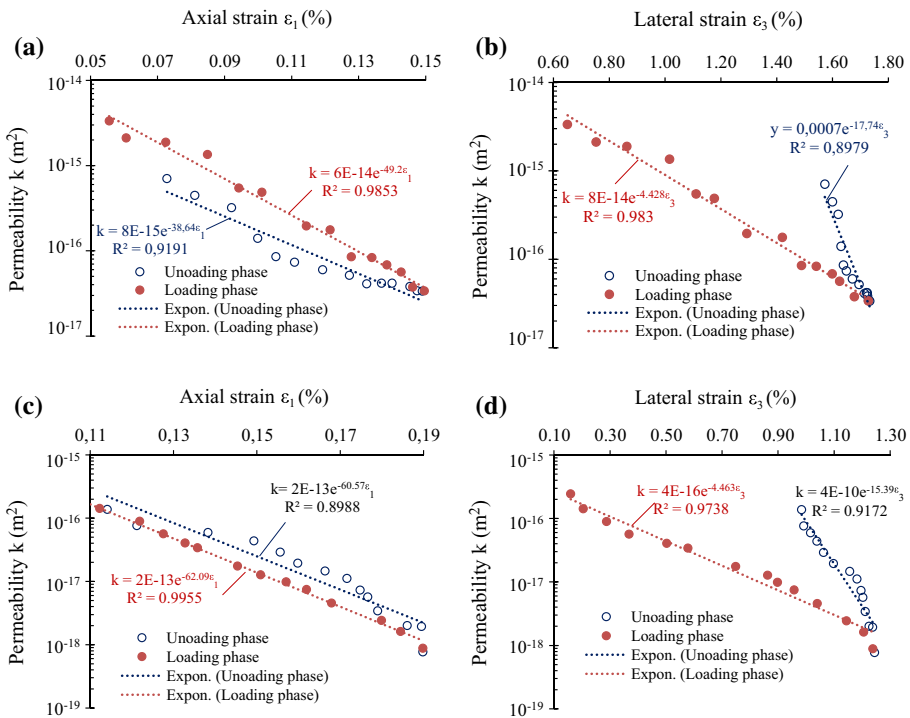


Fig. 7 Best-fitting models for permeability evolution as a function of axial and lateral strains, respectively, for both uniaxial cracked sample (a, b) and triaxial cracked sample with 2 MPa confining pressure (c, d)

power functions. In Fig. 6, we show the best-fitting models, with the determination coefficient (R^2) as criterion, for the evolution of permeability with the effective hydrostatic stress for both the uniaxial cracked sample and triaxial cracked one with 2 MPa confining pressure. And in Fig. 7, the evolution of permeability is expressed as a function of axial and lateral strains, respectively. The determination coefficient values given in these figures indicate that all the fitting models have a good performance for estimating the permeability of the cracked marble under hydrostatic compression.

As shown in Fig. 6, the best fitting of permeability evolution with the effective hydrostatic stress of the uniaxial cracked sample is given by the power model (Fig. 6a) while that of the triaxial cracked sample by the exponential model (Fig. 6b), for both the loading and unloading phases. In Fig. 7 and for both samples, one can see that the exponential model provides the best fitting of the relationship between the permeability and axial or lateral strains. Therefore, for the uniaxial cracked sample, the permeability evolution can be fitted by the power model in terms of effective stress but by the exponential model in terms of rock strains. For the triaxial cracked sample, the exponential model gives the best fitting of the permeability evolution in terms of both effective stress and strains. In this way, it is useful to formulate a unified fitting model for the permeability evolution of the uniaxial compression cracked sample. This unified model is expressed by:

$$k_{\text{uniaxial}} = a_1\sigma^{a_2} + b_1e^{b_2\cdot\varepsilon_1} + c_1e^{c_2\cdot\varepsilon_3} \tag{3}$$

And for the triaxial compression cracked sample, the following unified model can be obtained:

$$k_{\text{triaxial}} = a_1e^{a_2\cdot\sigma} + b_1e^{b_2\cdot\varepsilon_1} + c_1e^{c_2\cdot\varepsilon_3} \tag{4}$$

In these relations, k_{uniaxial} is the estimated permeability of the uniaxial cracked marble, and k_{triaxial} is that of the triaxial cracked one. σ , ε_1 and ε_3 are, respectively, the effective hydrostatic stress, the axial and lateral strains. a_1 , a_2 , b_1 , b_2 , c_1 , c_2 are the fitting parameters, which can be obtained from the experimental data. For instance, when $b_1 = 0$, $c_1 = 0$, Eqs. (3) and (4) reduce to the fitting models given in Fig. 6a, b, respectively. Similarly, when $a_1 = 0$, and either $b_1 = 0$ or $c_1 = 0$, Eqs. (3) and (4) recover the fitting models given in Fig 7.

The performance of the fitting models given in Eqs. (3) and (4) can be verified by the comparison between the experimental data and predicted results, as shown in Fig 8. After the determination of fitting parameters, the unified fitting models can be given in the following forms:

$$k_{\text{uniaxial}} = 3.13 \times 10^{-15}\sigma^{-0.29} - 3.04 \times 10^{-14}e^{-36.99\varepsilon_1} + 2.64 \times 10^{-14}e^{-16.96\varepsilon_3} \quad (R^2 = 0.9530) \tag{5}$$

$$k_{\text{triaxial}} = 7.63 \times 10^{-17}e^{-0.10\sigma} + 7.37 \times 10^{-14}e^{-68.57\varepsilon_1} + 1.52 \times 10^{-14}e^{-28.86\varepsilon_3} \quad (R^2 = 0.9705) \tag{6}$$

All the variables appearing in the above equations have the SI units.

7 Conclusion

In this paper, we have investigated the permeability evolution and deformation behavior of fractured marble samples under hydrostatic compression loading and unloading. The tested samples have previously been subjected to in cracking process in both uniaxial compression and triaxial compression tests with two different confining pressures. The spatial distribution and morphology of the induced cracks have been characterized by using the X-ray microtomographic imaging technique. In the uniaxial cracked sample, macroscopic splitting-type cracks were formed in the direction of the major compressive stress, while inclined diffuse shear-type cracks were observed in the triaxial cracked samples. The average aperture of the splitting cracks was greater than that of the shearing cracks.

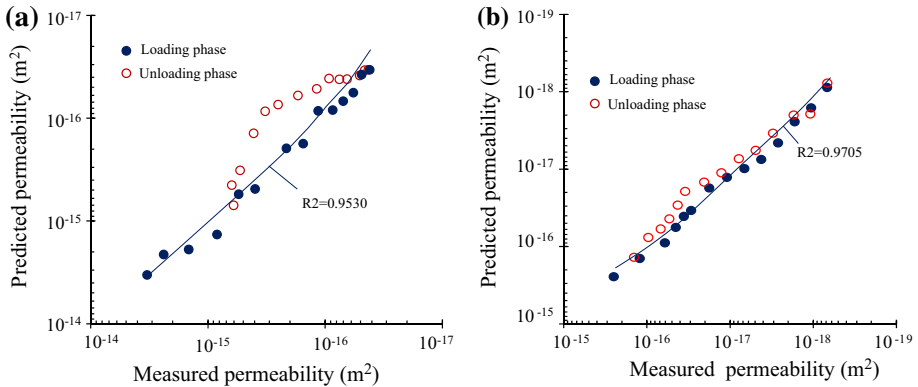


Fig. 8 Experimental verification of unified fitting models for permeability evolution in uniaxial cracked sample (a) and in triaxial cracked sample (b)

The permeability evolution of the cracked samples under hydrostatic loading and unloading is intimately related to the morphology of the induced cracks. The permeability of the sample with splitting cracks was more sensitive to applied effective hydrostatic stress than that of the samples with shearing cracks under low values of stress, say less than 15 MPa. Under high stress values, the permeability of the sample with splitting cracks exhibited a steady stage while that of the samples with shearing cracks showed a continuous decrease until 50 MPa. Further, the initial permeability (under 2 MPa effective stress) of the uniaxial cracked sample is one or two order of magnitude higher than that of the triaxial cracked samples, respectively, with 2 and 10 MPa confining pressures. Finally, for all three cracked samples, the permeability evolution exhibited an irreversible process between the loading and unloading phases due to the unilateral property of cracks.

For all three cracked samples, the deformation due to hydrostatic compression was strongly anisotropic due to the fact that the induced cracks are mainly oriented in the major compressive stress. Therefore, the lateral strains are much higher than the axial ones. Moreover, the lateral deformation of cracked samples exhibited very important irreversible strains due to the strong unilateral opening/closure behavior of cracks. Between the three samples, both axial and lateral strains of the uniaxial cracked sample are higher than those of the triaxial cracked samples.

Finally, we have applied the nonlinear regression method to formulate some best-fitting models for the permeability evolutions of cracked samples under hydrostatic compression. For the uniaxial cracked sample, the permeability evolution can suitably be fitted by the power model in terms of effective stress but by the exponential model in terms of rock strains. For the triaxial cracked sample, the exponential model gives the best fitting of the permeability evolution in terms of both effective stress and strains. We have finally combined these two functions to propose a unified fitting model for both samples in terms of effective stress and strains. The efficiency of the proposed model has been verified against the experimental data. In future works, it is wished to perform a deeper microstructural analysis of induced cracks in order to establish some quantitative correlations between the permeability evolution and cracks distribution.

Acknowledgments The authors would like to thank Dr. G. Hauss for his assistance in the realization of micro-tomographic analysis of the tested samples. Further, the data used in this paper are available from the corresponding author. Financial support from the NSFC (Nos. 51479193 and 51209085) and the “100 Talent Program” of the Chinese Academy of Sciences is gratefully acknowledged.

References

- Baghbanan, A., Jing, L.: Stress effects on permeability in a fractured rock mass with correlated fracture length and aperture. *Int. J. Rock Mech. Min. Sci.* **45**(8), 1320–1334 (2008)
- Berryman, J.G.: Effective stress for transport properties of inhomogeneous porous rock. *J. Geophys. Res. Solid Earth* **97**(B12), 17409–17424 (1992). doi:[10.1029/92JB01593](https://doi.org/10.1029/92JB01593)
- Boulon, M.J., Selvadurai, A.P.S., Benjelloun, H., Feuga, B.: Influence of rock joint degradation on hydraulic conductivity. *Int. J. Rock Mech. Min. Sci. Geomech. Abstr.* **30**(7), 1311–1317 (1993)
- Cappa, F., Guglielmi, Y., Rutqvist, J., Tsang, C.F., Thoraval, A.: Hydromechanical modelling of pulse tests that measure fluid pressure and fracture normal displacement at the Coaraze Laboratory site, France. *Int. J. Rock Mech. Min. Sci.* **43**(7), 1062–1082 (2006)
- Cook, N.G.W.: Natural joints in rock: mechanical, hydraulic and seismic behaviour and properties under normal stress. *Int. J. Rock Mech. Min. Sci.* **29**(3), 198–223 (1992). doi:[10.1016/0148-9062\(92\)93656-5](https://doi.org/10.1016/0148-9062(92)93656-5)
- Cornet, F., Morin, R.: Evaluation of hydromechanical coupling in a granite rock mass from a high-volume, high-pressure injection experiment: Le Mayet de Montagne, France. *Int. J. Rock Mech. Min. Sci.* **34**(3), 207. e201–207. e214 (1997)
- Hans, J., Boulon, M.: A new device for investigating the hydro-mechanical properties of rock joints. *Int. J. Numer. Anal. Methods Geomech.* **27**(6), 513–548 (2003)
- Henry, J.-P., Sibai, M.: Couplage hydromécanique dans les joints rocheux sous sollicitations normale: proposition de modélisation et comparaison avec l'expérience. *Expérimentation et Calcul en Génie Civil* **47**(54), 47–54 (1997)
- Jones, O.F.: A laboratory study of the effects of confining pressure on fracture flow and storage in carbonate rocks. *J. Petrol. Technol.* **27**, 21–27 (1975)
- Kishida, K., Kawaguchi, Y., Nakashima, S., Yasuhara, H.: Estimation of shear strength recovery and permeability of single rock fractures in shear-hold-shear type direct shear tests. *Int. J. Rock Mech. Min. Sci.* **48**(5), 782–793 (2011)
- Kwon, O., Kronenberg, A.K., Gangi, A.F., Johnson, B.: Permeability of Wilcox shale and its effective pressure law. *J. Geophys. Res. Solid Earth* **106**(B9), 19339–19353 (2001)
- Lee, H.S., Cho, T.F.: Hydraulic characteristics of rough fractures in linear flow under normal and shear load. *Rock Mech. Rock Eng.* **35**(4), 299–318 (2002)
- Li, B., Jiang, Y., Koyama, T., Jing, L., Tanabashi, Y.: Experimental study of the hydro-mechanical behavior of rock joints using a parallel-plate model containing contact areas and artificial fractures. *Int. J. Rock Mech. Min. Sci.* **45**(3), 362–375 (2008)
- Li, M., Bernabé, Y., Xiao, W.I., Chen, Z.Y., Liu, Z.Q.: Effective pressure law for permeability of E-bei sandstones. *J. Geophys. Res. Solid Earth* **114**(B7), n/a-n/a (2009)
- Lin, W.: Parametric analyses of the transient method of measuring permeability. *J. Geophys. Res. Solid Earth* **87**(B2), 1055–1060 (1982)
- Liu, Z., Shao, J., Xie, S., Secq, J.: Gas permeability evolution of clayey rocks in process of compressive creep test. *Mater. Lett.* **139**, 422–425 (2015)
- Myer, L.R.: Fractures as collections of cracks. *Int. J. Rock Mech. Min. Sci.* **37**(1–2), 231–243 (2000)
- Nøttinger, B.: The effective permeability of a heterogeneous porous medium. *Transp. Porous Media* **15**(2), 99–127 (1994)
- Nguyen, T.S., Selvadurai, A.P.S.: A model for coupled mechanical and hydraulic behaviour of a rock joint. *Int. J. Numer. Anal. Methods Geomech.* **22**(1), 29–48 (1998)
- Pyrak-Nolte, L.J., Morris, J.P.: Single fractures under normal stress: the relation between fracture specific stiffness and fluid flow. *Int. J. Rock Mech. Min. Sci.* **37**(1–2), 245–262 (2000)
- Raven, K.G., Gale, J.E.: Water flow in a natural rock fracture as a function of stress and sample size. *Int. J. Rock Mech. Min. Sci.* **22**(4), 251–261 (1985)
- Rutqvist, J., Stephansson, O.: The role of hydromechanical coupling in fractured rock engineering. *Hydrol. J.* **11**(1), 7–40 (2003)
- Selvadurai, A.P.S.: Normal stress-induced permeability hysteresis of a fracture in a granite cylinder. *Geofluids* **15**(1–2), 37–47 (2015)
- Selvadurai, A.P.S., Nguyen, T.S.: Mechanics and fluid transport in a degradable discontinuity. *Eng. Geol.* **53**(3–4), 243–249 (1999)
- Selvadurai, A.P.S., Selvadurai, P.A.: Surface permeability tests: experiments and modelling for estimating effective permeability. *Proc. R. Soc. Lond. A Math. Phys. Eng. Sci.* **466**(2122), 2819–2846 (2010)
- Sibai, M., Sotoudeh, M.H., Henry, J.P.: Etude expérimentale du couplage hydromécanique de joints rocheux. *Revue Française Géotechnologie* **81**, 33–39 (1997)
- Snow, D.T.: Rock fracture spacings, openings, and porosities. *J. Soil Mech. Foundations Div. Am. Soc. Civil. Eng.* **94**, 73–91 (1968)

- Souley, M., Lopez, P., Boulon, M., Thoraval, A.: Experimental hydromechanical characterization and numerical modelling of a fractured and porous sandstone. *Rock Mech. Rock Eng.* **48**(3), 1143–1161 (2015)
- Trimmer, D., Bonner, B., Heard, H.C., Duba, A.: Effect of pressure and stress on water transport in intact and fractured gabbro and granite. *J. Geophys. Res. Solid Earth* **85**(B12), 7059–7071 (1980)
- Tsang, Y.W., Witherspoon, P.A.: Hydromechanical behavior of a deformable rock fracture subject to normal stress. *J. Geophys. Res. Solid Earth* **86**(B10), 9287–9298 (1981)
- Tsang, Y.W., Witherspoon, P.A.: The dependence of fracture mechanical and fluid flow properties on fracture roughness and sample size. *J. Geophys. Res. Solid Earth* **88**(B3), 2359–2366 (1983)
- Witherspoon, P.A., Wang, J.S.Y., Iwai, K., Gale, J.E.: Validity of Cubic Law for fluid flow in a deformable rock fracture. *Water Resour. Res.* **16**(6), 1016–1024 (1980)
- Wong, L., Li, D., Liu, G.: Experimental studies on permeability of intact and singly jointed meta-sedimentary rocks under confining pressure. *Rock Mech. Rock Eng.* **46**(1), 107–121 (2013)
- Zhang, J., Standifird, W.B., Roegiers, J.C., Zhang, Y.: Stress-dependent fluid flow and permeability in fractured media: from lab experiments to engineering applications. *Rock Mech. Rock Eng.* **40**(1), 3–21 (2007)
- Zimmerman, R., Bodvarsson, G.: Hydraulic conductivity of rock fractures. *Transp. Porous Media* **23**(1), 1–30 (1996)
- Zou, L., Tarasov, B., Dyskin, A., Adhikary, D., Pasternak, E., Xu, W.: Physical modelling of stress-dependent permeability in fractured rocks. *Rock Mech. Rock Eng.* **46**(1), 67–81 (2013)